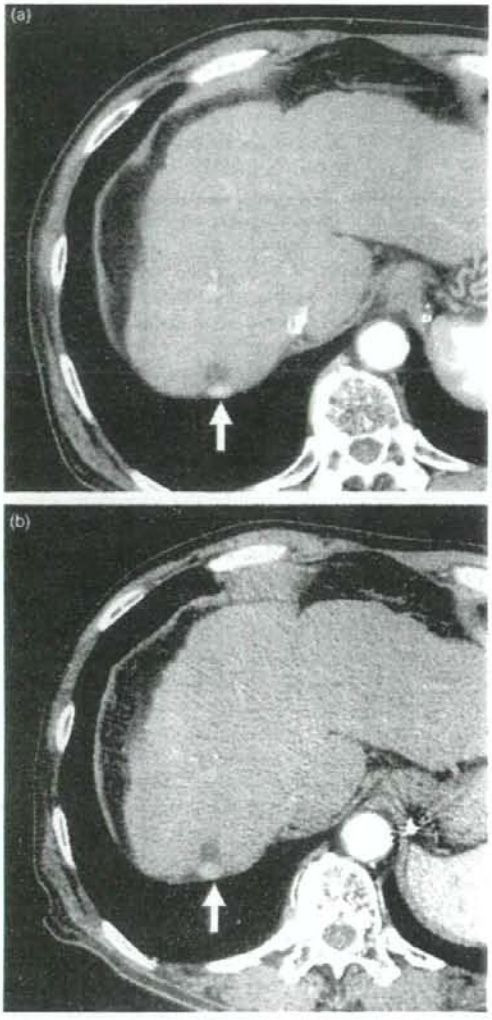

Fig. 2. Sixty-eight-year-old male, liver cirrhosis caused by alcohol abuse. (a) Contrast-enhanced computed tomography (CT) image on 10 March 2007. Contrast-enhanced CT image showed a hypervascular lesion (arrow) considered to be recurrence of hepatocellular carcinoma around the treated area. This lesion was not demonstrated by either non-contrast ultrasound (US) or contrast-enhanced US. (b) Contrast-enhanced CT image on 22 February 2008. Hypervascular lesion (arrow) did not show remarkable changes in form and size in comparison with that in the previous CT image. This hypervascular lesion was considered to be a vascular abnormality such as arterioportal communication.

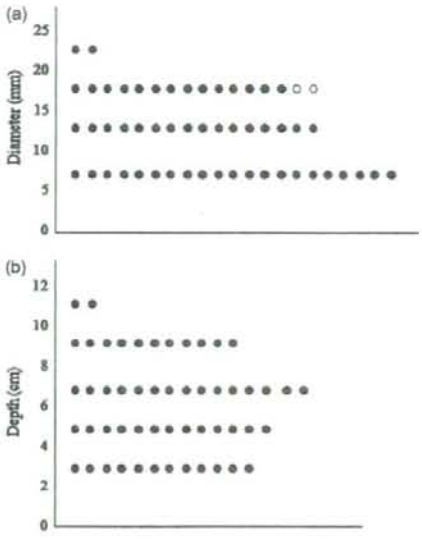

Fig. 3. (a) Distribution of hepatic lesions in relation to the diameter of the tumour. Twenty-one of the 55 lesions (38.2%) were < 10 mm. Closed circles: detected lesions [diameter measured by ultrasound (US)]. Open circles: undetected lesions (diameter measured by computed tomography). (b) Distribution of hepatic lesions in relation to the depth of the tumour location. Thirteen of the 55 lesions (23.6%) were located deeper than 8 cm from the skin surface. Two lesions undetected by contrast-enhanced US were not included because their depth was not measured on sonograms.

on contrast-enhanced CT images after the treatment. Thus, treatment effectiveness was confirmed on contrast-enhanced CT images and this was the evidence that the lesion contrast-enhanced US demonstrated was the lesion detected on contrast-enhanced CT. Six patients, each patient having one hypervascular lesion on contrast-enhanced CT, were treated by TACE alone because CT angiography showed more than three lesions in the liver. In the remaining seven lesions in six patients, six were diagnosed as non-HCC lesions. Two lesions were diagnosed as arterioportal communication by both CT angiography and contrast-enhanced US. Two lesions undetected by contrast-enhanced US were diagnosed as a vascular abnormality such as arterioportal communication because HCC was ruled out by CT angiography and the findings on subsequent contrast-enhanced CT showed no change in their clinical course, one case after 11 months and the other after 1 year (Fig. 2). One lesion was diagnosed as arteriovenous communication by contrast-enhanced US, and the other case with a benign lesion in alcoholic liver disease by a percutaneous needle biopsy. These six

lesions and one lesion with severe liver damage were followed up without any treatment, and the findings of the former six lesions on contrast-enhanced CT did not change during the clinical course of 8.4 ± 1.9 (5–14) months.

Discussion

Percutaneous US-guided treatments that require obvious demonstration of focal hepatic lesions on sonograms are minimally invasive and effective for HCC. However, a potential pitfall sometimes hinders the wider application of the technique, because visualization of focal hepatic lesions is not easy in cirrhotic patients (10, 11). To overcome this problem for the application of percutaneous US-guided treatments, some ingenious development is awaited.

As shown in the present study, the majority of ultrasonically unrecognized small hepatic lesions with a hypervascular appearance on contrast-enhanced CT were successfully demonstrated by contrast-enhanced US with Sonazoid™. Furthermore, the results suggested that our technique might be less dependent on the size or the location of the hepatic lesions.

Although all the hepatic lesions had a hypervascular appearance on contrast-enhanced CT, three of the 55 lesions showed equal enhancement on the early-phase sonograms. This might be explained by the saturation by contrast enhancement of the surrounding parenchyma owing to the inappropriate scan timing for the hepatic lesion, because the onset of contrast enhancement after the injection of the microbubble agent varies case by case and breath holding is sometimes inadequate. Furthermore, we had to observe early-phase images while searching for the lesions with positive enhancement by tilting the probe. Therefore, an inevitable delayed observation might account for the equal enhancement on the early-phase sonograms in these three hepatic lesions.

Meanwhile, the late-phase observation was relatively easy to perform, as with repeated observation it was possible to depict the negatively enhanced lesions in the liver parenchyma with homogeneous enhancement. However, detectability of hepatic lesions in the late phase was significantly lower than that in the early phase, and 11 of the 55 lesions had equal enhancement in the late phase. It is reported that Sonazoid™ microbubbles are captured by Kupffer cells in the liver (18), while retained intrahepatic microbubble circulation was found in approximately half of the subjects in the late phase in the present study. Therefore, the phase from 5 to 10 min after the injection of Sonazoid™ might not be produced by accumulated microbubbles alone, and the equal enhancement findings in some hepatic lesions in the late phase might be explained by the residual intravascular enhancement. In any event, observation both in the early phase and in the late phase would be necessary for detection of these hepatic lesions.

The previous study showed that Levovist (Schering AG, Berlin, Germany), a first-generation US contrast agent, improved the localization of ultrasonically unrecognized hypervascular lesions in the liver (12). However, the detection rate of 75% was lower than that with Sonazoid™. An appropriate imaging mode for Levovist was based on Doppler mode, which suffers from artefacts, and it requires the setting of regions of interest whose size vary inversely to the frame rate. In addition, contrast-enhanced US images were observed by a low frame rate of 4–8 Hz in the early phase and intermittent scanning with 1 frame/s in the late phase, imaging sequences suitable for Levovist. Thus, improved signal-to-noise ratio and real-time performance may be the advantages of our technique with Sonazoid™, which resulted in increased detectability of hepatic lesions in comparison with the results using Levovist. Another study showed that RFA was sufficiently achieved using Sonazoid™ for undetected lesions by conventional US (19). However, that study had some differences from ours, because it included large-sized tumours and the use of a combined method with low acoustic power and high acoustic power according to the phase. Although an optimal acoustical condition for Sonazoid™ has still not been established, our technique under a low-MI condition throughout the examination may be more simple and convenient. Obviously, the establishment of appropriate imaging sequences would be helpful for the standardization and popularization of contrast-enhanced US with Sonazoid™.

We failed to demonstrate two focal hepatic lesions in our study, which were fortunately considered to be arterioportal communications. In fact, there were five patients with vascular abnormalities, so-called 'pseudo-lesions', that sometimes confuse the differentiation from hypervascular HCC on contrast-enhanced CT (21–23). The reasons for detection failure of these lesions may be the difficulty of sonographical demonstration because of the location and/or the pathological property of the vascular abnormality. Although our technique achieved quite a high detection rate for malignant hepatic lesions, improvement in diagnostic ability for such vascular abnormalities would be a worthwhile mission for contrast-enhanced US development in the near future.

There was one benign hepatic lesion histologically proven in one patient with alcoholic liver disease. It is

Liver International (2008)

known that hypervascular hepatic lesions do not always reflect the fact that the final diagnosis of the nodule is HCC in heavy drinkers (24). The ring-shaped appearance on liver-specific contrast-enhanced sonograms with Levovist is reported to be a useful sign for the diagnosis of a benign nodule in heavy drinkers (25). However, the benign lesion in the present study did not show this sign in the late phase. Although this might be explained by the very small size of the lesion in which the ring-shaped appearance was hard to recognize and/or the difference of microbubble property between Levovist and Sonazoid™, further studies would be needed to investigate this issue.

CT-guided needle puncture is also an effective method for hepatic tumours not recognized by US examination (26–29). However, it is not an easy procedure, and it requires radiation exposure and is time consuming. As contrast-enhanced US with Sonazoid™ could provide quite sufficient detectability of ultrasonically unrecognizable hepatic lesions, the application of CT-guided treatment may be confined to cases not demonstrated by contrast-enhanced US.

Cost, time and manpower are not negligible aspects to discuss the value of physical examination. As for the cost of contrast agent, one vial of Sonazoid™ (about US$100) is usually enough for one patient, because 2.0 ml of Sonazoid™ solution is available by one vial and each injection was applied at a dose of 0.0075 ml/kg in our method. Next, contrast-enhanced US examination is not a costless work, because it needs an assistant for the preparation and injection of a contrast agent, in addition to the US operator. Furthermore, as about 10-min observation was required for both the early and the late phase in our study, contrast-enhanced US may not be as brief as conventional US. However, the benefit and safety of contrast-enhanced US with Sonazoid™ would outweigh the cost manpower and time required in this procedure.

The present study has the limitation that the diagnosis of all hepatic lesions was not proven histologically. The European Association for the Study of the Liver has documented that nodules larger than 2 cm with an arterial hypervascular pattern by two imaging techniques are diagnosed as HCC without pathological findings, and sampling error could not be denied in the needle biopsy for small hepatic lesions (3, 30). Therefore, histological proof for all hepatic lesions may not be indispensable in our study. However, various kinds of hypervascular hepatic tumours such as haemangioma or focal nodular hyperplasia might have been included, although their diagnosis on contrast-enhanced CT was HCC. A second limitation was that there were no additional lesions detected by contrast-enhanced US, because the observation of contrast enhancement was limited to the tumour area estimated by contrast-enhanced CT. In fact, we had six patients treated by TACE alone because CT angiography following contrast-enhanced US showed more than one lesion that was presented on contrast-enhanced CT in the liver. Although the early-phase observation for multiple hepatic lesions may be difficult, scanning for other areas of the liver in the late phase might be helpful for detecting additional lesions as hypo-enhancement lesions. As these six patients were, after all, treated not by US-guided treatment but by TACE, demonstration of additional lesions might not affect the therapeutic strategy for them. However, this point may be improved with an increase in the detectability of hepatic lesions by contrast-enhanced US.

In conclusion, the detection rate of ultrasonically unrecognized hypervascular HCC was improved by contrast-enhanced US with Sonazoid™. This technique may allow the wider application of percutaneous US-guided treatments, which are minimally invasive procedures, in patients with HCC.

References

1. Bosch FX, Ribes J, Borras J. Epidemiology of primary liver cancer. *Semin Liver Dis* 1999; **19**: 271–85.
2. Okuda K. Hepatocellular carcinoma. *J Hepatol* 2000; **32**: 225–37.
3. Bruix J, Sherman M, Llovet JM, *et al.* Clinical management of hepatocellular carcinoma. Conclusions of the Barcelona-2000 EASL conference. European Association for the Study of the Liver. *J Hepatol* 2001; **35**: 421–30.
4. Ryu M, Shimamura Y, Kinoshita T, *et al.* Therapeutic results of resection, transcatheter arterial embolization and percutaneous ethanol injection in 3225 patients with hepatocellular carcinoma: a retrospective multicenter study. *Jpn J Clin Oncol* 1997; **27**: 251–7.
5. Livraghi T, Bolondi L, Lazzaroni S, *et al.* Percutaneous ethanol injection in the treatment of hepatocellular carcinoma in cirrhosis. A study on 207 patients. *Cancer* 1992; **69**: 925–9.
6. Goldberg SN, Gazelle GS, Solbiati L, Rittman WJ, Mueller PR. Radiofrequency tissue ablation: increased lesion diameter with a perfusion electrode. *Acad Radiol* 1996; **3**: 636–44.
7. Giorgio A, Tarantino L, de Stefano G, *et al.* Percutaneous sonographically guided saline-enhanced radiofrequency ablation of hepatocellular carcinoma. *Am J Roentgenol* 2003; **181**: 479–84.

8. Lencioni RA, Allgaier HP, Cioni D, *et al.* Small hepatocellular carcinoma in cirrhosis: randomized comparison of radiofrequency thermal ablation versus percutaneous ethanol injection. *Radiology* 2003; **228**: 235–40.
9. Ebara M, Okabe S, Kita K, *et al.* Percutaneous ethanol injection for small hepatocellular carcinoma: therapeutic efficacy based on 20-year observation. *J Hepatol* 2005; **43**: 458–64.
10. Takayasu K, Muramatsu Y, Asai S, *et al.* CT fluoroscopy-assisted needle puncture and ethanol injection for hepatocellular carcinoma: a preliminary study. *Am J Roentgenol* 1999; **173**: 1219–24.
11. Sato M, Watanabe Y, Tokui K, *et al.* CT-guided treatment of ultrasonically invisible hepatocellular carcinoma. *Am J Gastroenterol* 2000; **95**: 2102–6.
12. Maruyama H, Kobayashi S, Yoshizumi H, *et al.* Application of percutaneous ultrasound-guided treatment for ultrasonically invisible hypervascular hepatocellular carcinoma using microbubble contrast agent. *Clin Radiol* 2007; **62**: 668–75.
13. Goldberg BB. *Ultrasound Contrast Agents*. London: Martin Dunitz Ltd, 1997; 169.
14. Morel DR, Schwieger I, Hohn L, *et al.* Human pharmacokinetics and safety evaluation of SonoVue, a new contrast agent for ultrasound imaging. *Invest Radiol* 2000; **35**: 80–5.
15. Maruyama H, Matsutani S, Saisho H, Mine Y, Yuki H, Miyata K. Extra-low acoustic power harmonic images of the liver with Perflutren: novel imaging for real-time observation of liver perfusion. *J Ultrasound Med* 2003; **22**: 931–8.
16. von Herbay A, Vogt C, Willers R, Haussinger D. Real-time imaging with the sonographic contrast agent SonoVue: differentiation between benign and malignant hepatic lesions. *J Ultrasound Med* 2004; **23**: 1557–68.
17. Marelli C. Preliminary experience with NC100100, a new ultrasound contrast agent for intravenous injection. *Eur Radiol* 1999; **9**(Suppl. 3): S343–6.
18. Watanabe R, Matsumura M, Munemasa T, Fujimaki M, Suematsu M. Mechanism of hepatic parenchyma-specific contrast of microbubble-based contrast agent for ultrasonography: microscopic studies in rat liver. *Invest Radiol* 2007; **42**: 643–51.
19. Numata K, Morimoto M, Ogura T, *et al.* Ablation therapy guided by contrast-enhanced sonography with sonazoid for hepatocellular carcinoma lesions not detected by conventional sonography. *J Ultrasound Med* 2008; **27**: 395–406.
20. Maruyama H, Matsutani S, Okugawa H, *et al.* Microbubble disappearance-time is the appropriate timing for liver-specific imaging after injection of Levovist. *Ultrasound Med Biol* 2006; **32**: 1809–15.
21. Yu JS, Kim KW, Sung KB, *et al.* Small arterial-portal venous shunts: cause of pseudolesions at hepatic imaging. *Radiology* 1997; **203**: 737–42.
22. Kim TK, Choi BI, Han JK, *et al.* Nontumorous arterioportal shunt mimicking hypervascular tumor in cirrhotic liver: two-phase spiral CT findings. *Radiology* 1998; **208**: 597–603.
23. Brancatelli G, Baron RL, Peterson MS, *et al.* Helical CT screening for hepatocellular carcinoma in patients with cirrhosis: frequency and causes of false-positive interpretation. *Am J Roentgenol* 2003; **180**: 1007–14.
24. Kim SR, Maekawa Y, Ninomiya T, *et al.* Multiple hypervascular liver nodules in a heavy drinker of alcohol. *J Gastroenterol Hepatol* 2005; **20**: 795–9.
25. Maruyama H, Matsutani S, Kondo F, *et al.* Ring-shaped appearance on liver-specific image with Levovist: a characteristic enhancement pattern for hypervascular benign nodule in the liver of heavy drinkers. *Liver Int* 2006; **26**: 688–94.
26. Schweiger GD, Brown BP, Pelsang RE, *et al.* CT fluoroscopy: technique and utility in guiding biopsies of transiently enhancing hepatic masses. *Abdom Imaging* 2000; **25**: 81–5.
27. Shibata T, Iimuro Y, Yamamoto Y, *et al.* CT-guided transthoracic percutaneous ethanol injection for hepatocellular carcinoma not detected with US. *Radiology* 2002; **223**: 115–20.
28. Kirchner J, Kickuth R, Laufer U, *et al.* CT fluoroscopy-assisted puncture of thoracic and abdominal masses: a randomized trial. *Clin Radiol* 2002; **57**: 188–92.
29. Adam A, Hatzidakis A, Hamady M, *et al.* Percutaneous coil placement prior to radiofrequency ablation of poorly visible hepatic tumors. *Eur Radiol* 2004; **14**: 1688–91.
30. Nakashima T, Kojiro M. *Hepatocellular Carcinoma*. Tokyo: Springer-Verlag, 1987.

Hemodynamic Features of Gastrorenal Shunt:
A Doppler Study in Cirrhotic Patients with Gastric Fundal Varices[1]

Hitoshi Maruyama, MD, Hidehiro Okugawa, MD, Hiroaki Yoshizumi, MD, Satoshi Kobayashi, MD, Osamu Yokosuka, MD

Rationale and Objectives. Little is known about the hemodynamics of gastrorenal shunt (GRS), a major drainage route of gastric fundal varices (FV), in patients with FV. The aim of this study was to clarify the hemodynamic features of GRS on Doppler sonography in relation to the grading and bleeding of FV.

Materials and Methods. The study subjects consisted of 69 cirrhotic patients with FV. Diameter, flow velocity (FVe), and flow volume (FVo) of GRS were measured by Doppler ultrasound (US). The detection rate was compared to contrast-enhanced computed tomography (CECT), and percutaneous transhepatic portography (PTP) was used in six patients without GRS on CECT.

Results. The use of CECT detected GRS in 60 of 69 patients, and US, 58 of 69 patients. A false-negative result for detecting GRS on both CECT and US was found in one patient after PTP. The diameter, FVe, and FVo of GRS increased according to the endoscopic grade of FV: F1 (7.2 ± 1.3 mm, 9.8 ± 1.1 cm/s, 358.3 ± 123.4 ml/min), F2 (9.9 ± 3.3 mm, 12.8 ± 5.1 cm/s, 701.7 ± 411.3 ml/min), and F3 (11.8 ± 2.4 mm, 17.9 ± 8.3 cm/s, 1706.6 ± 989.5 ml/min). A significant difference was seen between F1 and F3 (diameter, $P = .0022$; FVe, $P = .0133$; FVo, $P = .0007$) and between F2 and F3 (FVe, $P = .0112$; FVo, $P < .0001$). FVe of GRS was significantly higher in bleeders (16.7 ± 8.1 cm/s) than in nonbleeders (12.2 ± 5.4 cm/s, $P = .017$), whereas the diameter and FVo were not significant.

Conclusion. Hemodynamics of GRS on Doppler sonograms reflected the grading and bleeding of FV. Doppler US may be valuable as a noninvasive method to evaluate the severity of FV.

Key Words. Gastric varices; portal hypertension; Doppler ultrasound; gastrorenal shunt.

Gastric fundal varices (FV) are known to be a considerable complication in patients with portal hypertension (1,2). Although the rates of bleeding for FV have been reported to be lower than those for esophageal varices (EV), rupture from FV sometimes results in serious consequences in the clinical course (3,4). Certain treatment methods using endoscopy, interventional techniques, and surgical procedures have been introduced for FV (5–19). However, a few studies have reported risk factors for FV bleeding, and hemodynamic features associated with FV bleeding have not been clarified (1,20,21).

There are a number of inflow vessels into FV: the left gastric, posterior gastric, and short gastric veins (22–26). The main outflow pathway in the majority of FV is the gastrorenal shunt (GRS), and the blood flow manner of GRS may represent the clinical condition of FV. Watanabe et al. (25), using the percutaneous transhepatic portography (PTP) technique, reported that the diameter of the GRS depended on the severity of FV. However, that study was based on a nonphysiologic condition using portal venous catheterization, and it lacked quantitative assessment. Little is known about

Acad Radiol 2008; 15:1148–1154

[1] From the Department of Medicine and Clinical Oncology, Chiba University Graduate School of Medicine, 1-8-1, Inohana, Chuou-ku, Chiba, 260-8670, Japan. Received December 11, 2007; accepted March 8, 2008. **Address correspondence to:** H.M. e-mail: maru-cib@umin.ac.jp

doi:10.1016/j.acra.2008.03.008

the physiologic hemodynamic features of the GRS in patients with FV.

Pulsed and color Doppler ultrasound (US) allows the real-time observation of the portal hemodynamics in patients with portal hypertension, repeatedly and noninvasively, with quantitative evaluation (27–29). The recent study demonstrated the portal systemic shunt through the renal vein on sonograms (30,31). Using this technique, we designed the present study to investigate the physiology of GRS in patients with FV. The aim of this study was to clarify the hemodynamics of GRS on Doppler sonography in relation to the grading and bleeding of FV.

MATERIALS AND METHODS

Patients

There were 76 consecutive patients with FV confirmed by endoscopic examination in our hospital between December 1999 and August 2007. Among them, seven patients received endoscopic treatment before the hemodynamic evaluation using US because of active bleeding from the FV. Therefore, 69 patients with FV formed the subject group in this retrospective study. They consisted of 36 men and 33 females, aged 41 to 80 years (mean age, 61.5 ± 8.9), and their body mass index (BMI) was 22.5 ± 4.1 kg/m^2 (range, 16.8 to 30.9). All of them had liver cirrhosis diagnosed on the basis of imaging findings, histologic findings, clinical symptoms, and biochemistry findings. The cause of liver cirrhosis was viral in 44 patients (hepatitis virus C, 40; hepatitis virus B, 4), alcohol in 9, nonalcoholic steatohepatitis (NSAH) in 3, autoimmune in 1, primary biliary cirrhosis in 3, and cryptogenic in 9. The severity of liver dysfunction, as classified according to the Child-Pugh scoring system (32), was A in 30, B in 26, and C in 13 patients. Eighteen patients had hepatocellular carcinoma (HCC), which was being controlled by nonsurgical treatment, and none had thrombus or tumor thrombus in the portal vein on US and contrast-enhanced computed tomography (CECT). Informed written consent was obtained from all patients. The preliminary step for ethics committee in our hospital deemed this retrospective study as appropriate design without approval.

Endoscopy

Endoscopic findings of FV and EV were classified according to the General Rules for Recording Endoscopic Findings set by the Japan Research Society for Portal Hypertension (33)—F1 (straight), F2 (winding), and F3 (nodule-beaded), corresponding to the grades of small, medium, and large, respectively. The grades of FV were F1 in 10, F2 in 38, and F3 in 21 patients; 24 of the FV patients were accompanied by EV, F1 in 14, and F2 in 10. All patients had primary FV, and there was no secondary FV developed after the obliteration of esophageal varices. Twenty patients were bleeders—6 were confirmed by emergency endoscopy and 14 were confirmed by clinical symptoms of hematemesis or melena. The former six bleeders received endoscopic cyanoacrylate injection therapy to attain hemostasis after the US examination. The latter 14 bleeders underwent endoscopic examination within 2 weeks after their symptoms, and another cause for gastrointestinal bleeding was not found except for FV. The remaining 49 were nonbleeders with no history of hematemesis or melena.

Contrast-enhanced Computed Tomography

CECT with dynamic study was performed in all patients using either a Somatom Plus 4 (Siemens Medical Systems, Erlangen, Germany) or a Lightspeed Ultra16 (GE Medical Systems, Milwaukee, WI) with the injection of 100 ml of contrast medium at 3 ml/s from the antecubital vein via mechanical power injector. The acquisition parameters of computed tomographic examination were 140 kV, 200 mA, scan time 0.75 s/rotation, and beam pitch 1.5 for Somatom Plus 4, and 120 kV, 350 mA (CT-AEC), scan time 0.8 s/rotation, beam pitch 1.375, and collimation 0.625 mm for Lightspeed Ultra16. Scanning was performed with a 30-s delay between contrast administration and start of scanning for the hepatic artery−dominant phase, 80-s delay for the portal vein−dominant phase, and 180-s delay for the equilibrium phase. The computed tomographic image was evaluated by one of the authors (H.O.).

Ultrasound

Equipment and settings.—The US systems used in the present study were SSA-380A, 390A, and 770A (Toshiba, Tokyo, Japan), which were the high-end systems during the study period, with a 3.75-MHz convex probe. The imaging modes were gray-scale B-mode US, pulsed Doppler US, and color flow imaging. Pulsed Doppler US was used for the measurement of mean flow velocity (FVe, centimeters per second) and mean flow volume (FVo, milliliters per minute), with sampling width corresponding to the maximum diameter of the vessel and at an angle less than 60° between the US beam

and the vessel. Color flow imaging was done with an optimal level of gain and at 65 dB of dynamic range, and these settings were used in all examinations. US examination was performed in the spine position and a fasting state of over 6 hours (except for the bleeders) and patients were asked to breathe normally.

Demonstration of gastrorenal shunt.—At first, the left renal vein was detected with a long-axis view on the sonogram by transverse scan in the middle part of the abdomen. Then, the probe was turned clockwise approximately 90° for a sagittal scan at the left side of the abdominal aorta. The GRS on the sonogram was defined as the vessel that communicated with the left renal vein running beside the abdominal aorta with a long-axis view. When the GRS was not observed on the image, the probe was tilted gently from side to side. After the presence and direction of blood flow were confirmed by color flow imaging, the maximum diameter of GRS was measured on the gray-scale sonogram and blood flow was measured by pulsed Doppler US. The sensitivity and specificity of US in detecting GRS for CT were evaluated. All US examinations were performed by one of the authors (H.M., a specialist in gastroenterology and hepatology with a 14-year career with Doppler US), and all digitally stored sonograms on the magneto-optical disk were reviewed at a later date by two of the authors (S.K. and H.Y.). A second US examination within 1 week (4 to 7 days) after the initial one was done in 13 patients who had sufficient time before prophylactic treatment, and intraobserver variability for the measurement results of GRS was calculated. US examinations were performed before the treatment for FV in all patients.

Percutaneous Transhepatic Portography

Portal vein catheterization was performed by means of a US-guided procedure (34), and a portogram was obtained during the injection of contrast medium into the splenic hilum.

Statistical Analysis

All results were expressed as mean ± standard deviation or percentage. All statistical analysis was performed using the StatView for Windows (version 5.0J; SAS Institute Inc., Cary, NC). Fisher's protected least-significant difference (PLSD) was used to compare the diameter, FVe, and FVo of GRS with the grade of FV, Child's classification, or causes of liver cirrhosis, and the Mann-Whitney *U*-test was used to compare the diameter, FVe, and FVo of GRS with the presence of EV or bleeding of FV. Significance was taken at $P < .05$ for all tests.

RESULTS

Comparison of the Detection Rate of Gastrorenal Shunt Between Ultrasound and Contrast-enhanced Computed Tomography

On US, the sagittal plane demonstrated a long-axis view of the GRS from the cranial and dorsal side to the caudal and ventral side, which connects into the left renal vein (Fig. 1). GRS was detected by US in 58 patients (58 of 69, 84.1%) and by CECT in 60 patients (60 of 69, 87%). US failed to detect GRS in two CECT-positive patients, likely because of excessive gas in the gastrointestinal tract. The sensitivity and specificity of US in detecting CECT detected GRS were 96.7% and 100%, respectively.

Forty-two patients required curative treatment for FV—20 with a bleeding history and 22 who hoped for prophylaxis for middle-sized or large FV. Drainage route of FV was clearly demonstrated on CECT and/or US in 36 patients—the GRS in 35 and inferior phrenic vein (IPV) in one. The other 6 patients for whom the drainage route was not demonstrated on the images underwent PTP for pretreatment portal hemodynamics evaluation. The portogram revealed the presence of GRS with a partially narrowed appearance in one patient (see Fig. 2), and the remaining five patients had other vessels for the drainage route of FV—the azygos vein in three and the IPV in two. Therefore, 39 patients underwent balloon-occluded retrograde transvenous obliteration (B-RTO) from the drainage routes of FV (GRS in 36 patients and IPV in 3 patients), and the other 3 patients were followed up without additional treatment.

Hemodynamic Features of Gastrorenal Shunt on the Sonograms

GRS on the sonograms showed flow direction continuously toward the left renal vein in 53 patients, but a to-and-fro appearance was observed in the other five patients (F1 in 2 and F2 in 3; Fig. 3).

The diameter, FVe, and FVo of GRS increased according to the endoscopic grade of FV in 53 patients without a to-and-fro appearance (Table 1): F1 (7.2 ± 1.3 mm, 9.8 ± 1.1 cm/s, 358.3 ± 123.4 ml/min), F2 (9.9 ± 3.3 mm, 12.8 ± 5.1 cm/s, 701.7 ± 411.3 ml/min), and F3 (11.8 ± 2.4 mm, 17.9 ± 8.3 cm/s, 1706.6 ± 989.5 ml/min). A

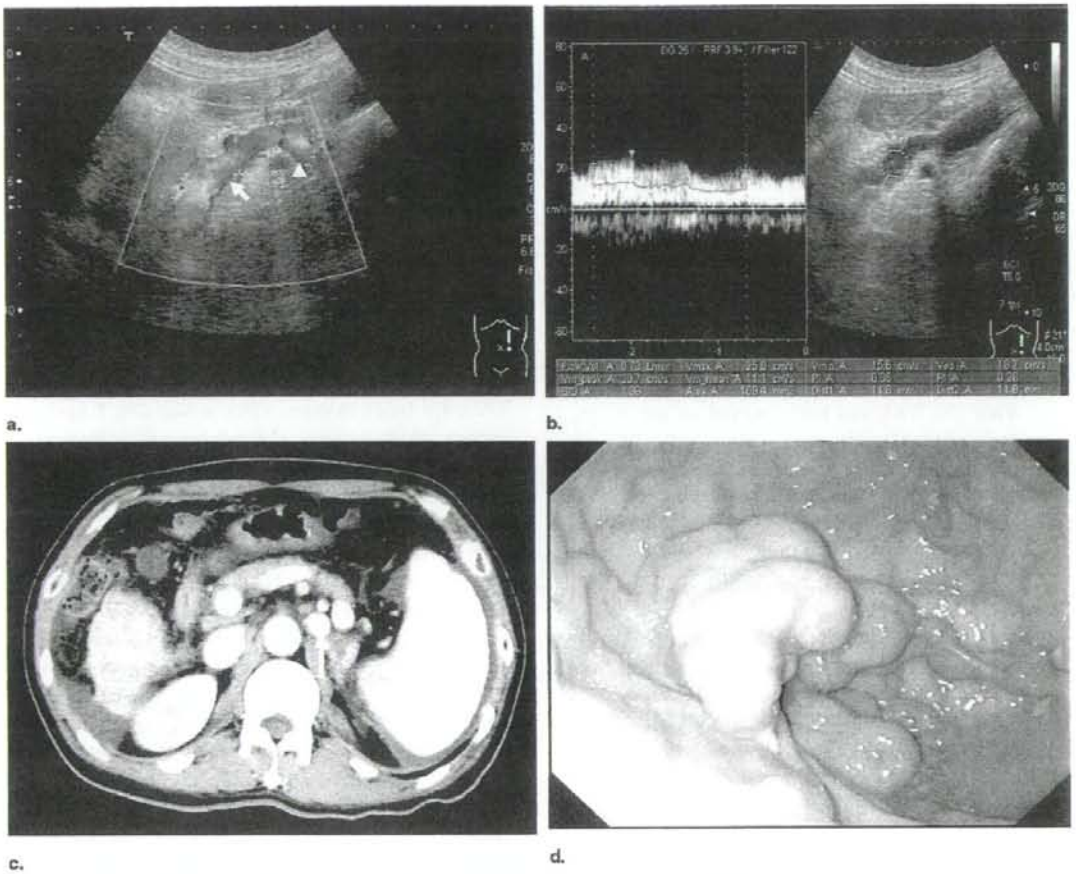

Figure 1. Demonstration of gastrorenal shunt (GRS) on Doppler ultrasound and contrast-enhanced computed tomography (CECT) images in patient with gastric fundal varices (52-year-old man). **(a)** The sagittal plane of the color Doppler sonogram demonstrated a long-axis view of GRS (*arrow*) from the cranial and dorsal side to the caudal and ventral side, which connects into the left renal vein (*arrowhead*) with a flow direction continuously toward the left renal vein. **(b)** Pulsed Doppler. Flow velocity and flow volume were measured by the pulsed Doppler method. **(c)** CECT. CECT demonstrated GRS at the left side of the abdominal aorta (*arrow*). **(d)** Endoscopy. This patient had large-grade FV (F3).

significant difference was seen between F1 and F3 (diameter, $P = .0022$; FVe, $P = .0133$; FVo, $P = .0007$; Fisher's PLSD) and between F2 and F3 (FVe, $P = .0112$; FVo, $P < .0001$; Fisher's PLSD). However, the diameter, FVe, and FVo showed no significant difference between patients with EV and patients without EV, and in relation to the causes of liver cirrhosis. FVe of GRS was significantly higher in bleeders (16.7 ± 8.1 cm/s) than in nonbleeders (12.2 ± 5.4 cm/s, $P = .017$, Mann-Whitney *U*-test; Table 2), whereas the diameter and FVo were not significant. The diameter, FVe, and FVo of GRS also increased according to the progression of Child's classification: A (9.0 ± 2.4 mm, 12.2 ± 5.5 cm/s, 819.9 ± 521.6 ml/min), B (10.3 ± 3.3 mm, 13.6 ± 4.9 cm/s, 791.3 ± 578.4 ml/min), and C (11.9 ± 2.8 mm, 19.7 ± 9.9 cm/s, 1610 ± 996.7 ml/min). FVe between Child A and C ($P = .015$, Fisher's PLSD) and FVo between Child A and C ($P = .023$, Fisher's PLSD) and between B and C ($P = .035$, Fisher's PLSD) were significantly different. Intraobserver variability for the measurement results of GRS was 5.2% for diameter, 7.7% for FVe, and 9.3% for FVo.

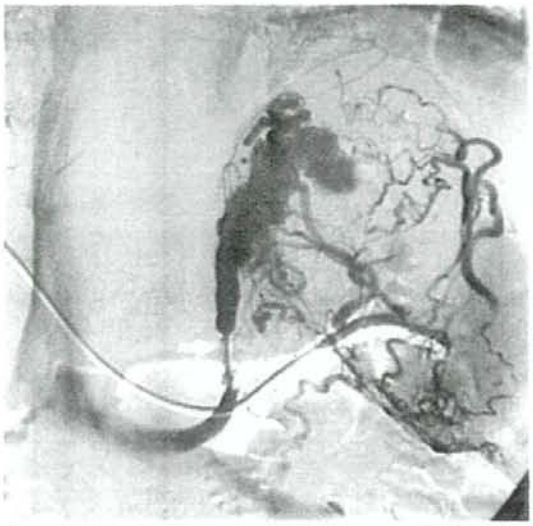

Figure 2. A portogram showing a gastrorenal shunt (GRS) with a linear stricture (*arrow*). Neither ultrasound nor contrast-enhanced computed tomography demonstrated GRS in this case.

DISCUSSION

The present study is probably the first to report on the physiologic hemodynamics of GRS, a main outflow route of FV, in relation to the condition of FV. Gray-scale US detected GRS using a longitudinal scan with a long-axis view at the left side of the abdominal aorta, and Doppler US dramatically demonstrated real-time blood flow imaging. Quantitative assessment of the hemodynamics of GRS was successfully conducted by this method in cirrhotic patients with FV.

As for the detection rate of GRS, US showed a similar rate to that of CECT for the visualization of GRS. Although there is little doubt that three-dimensional computed tomographic images can be useful for the detection of GRS (22), excessive exposure to x-rays has become a major problem worldwide. Application of CECT only for the purpose of detecting GRS in patients with FV may be limited to those in whom GRS is not detected by US. However, as visualization on the sonograms depends on the physical size of the patients, the detectability of GRS may vary by race. Contrast-enhanced US with microbubble contrast agents might be a worthwhile option for improving the detectability of the blood flow of GRS (29).

We had nine cases whose GRS was not demonstrated on CECT and US images. Portal venous hemodynamics was examined by PTP in six of them, and the GRS in one case had a partial linear stricture that was considered to be the reason for the detection failure on US and CECT. Although such a case might be rare in clinical practice, advancement of the balloon catheter without this information beforehand would be a dangerous maneuver during B-RTO. If US/CT does not show the existence of GRS, PTP or arterial portography should be performed for the confirmation of the presence and patency of GRS. GRS might be present in our three other cases without GRS according to CECT and US. In addition, our method may need to be compared with magnetic resonance imaging, which is also useful for the evaluation of portal hemodynamics.

B-RTO has received considerable attention recently as an effective method for the treatment of FV (8–10). Because the application of this technique depends on the presence of GRS, our method may prove useful for deciding the therapeutic strategy in patients with FV. In addition, measurement of the diameter of GRS might help in balloon size selection for the GRS occlusion during B-RTO. The IPV is also a drainage route to which B-RTO can be applied in patients with FV, although it is less common than GRS (9,10). The present study had three cases with IPV, and only one of them was visible by US. Although there may be an anatomic reason for missing these, the poor visualization of IPV on a sonogram is a shortcoming of our method.

Flow velocity and flow volume of GRS corresponded to the endoscopic grade of FV and liver function, and these results may suggest that the hemodynamics of GRS depend on the development of hepatofugal collateral blood flow. However, there was no significant difference in the parameters of GRS between small-grade FV (F1) and medium-grade FV (F2). This might be explained by the exponential hemodynamic change between F2 and F3 in the progressing course of FV from F1 to F3. However, as a small number of patients with F1 grade might affect this statistical result, further study would be necessary to clarify this point.

Meanwhile, the measured parameters of GRS by Doppler US did not show any significant difference between patients with EV and patients without EV, and in relation to the causes of cirrhosis. The hemodynamics of GRS might be specific to the FV itself, regardless of the presence of the EV and the causes of cirrhosis.

Our study had five cases with GRS in which the blood flow direction appeared as to-and-fro on color Doppler imaging. This physiologic phenomenon has not been doc-

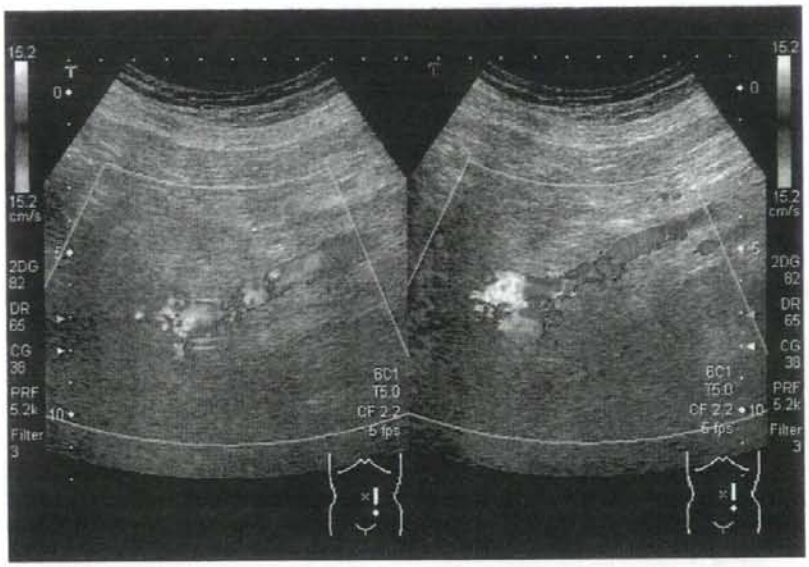

Figure 3. Color Doppler (72-year-old man with medium-grade gastric fundal varices [F2]). The sagittal plane of the color Doppler sonogram showed gastrorenal shunt with a to-and-fro appearance.

Table 1
Hemodynamics in the Gastrorenal Shunt (GRS) in Relation to the Grade of Gastric Fundal Varices

	GRS (mean ± SD)		
FV	Diameter (mm)	FVe (cm/s)	FVo (mL/m)
F1	7.2 ± 1.3*	9.8 ± 1.1‡	358.3 ± 123.4**
F2	9.9 ± 3.3†	12.8 ± 5.1§	701.7 ± 411.3††
F3	11.8 ± 2.4*†	17.9 ± 8.3‡§	1706.6 ± 989.5**††

FVe: flow velocity; FVo: flow volume.
*P = .0022; †P = .0515; ‡P = .0133; §P = .0112; **P = .0007; ††P < .0001 (Fisher's PLSD).

Table 2
Hemodynamics in the Gastrorenal Shunt (GRS) in Relation to the Bleeding of Gastric Fundal Varices

	GRS (mean ± SD)		
	Diameter (mm)	FVe (cm/s)	FVo (mL/m)
Nonbleeder	10.2 ± 3.5*	12.2 ± 5.4†	843.8 ± 810.3‡
Bleeder	10.3 ± 2.5*	16.7 ± 8.1†	1187.1 ± 914.2‡

FVe: flow velocity; FVo: flow volume.
*‡Nonsignificant; †P = .017 (Mann-Whitney U-test).

umented elsewhere, and it may not be demonstrated except by Doppler US examination. The authors speculate that low portal venous pressure and/or additional hemodynamic factors such as the presence of IPV might be connected with this phenomenon, although the cause for this hemodynamic remains to be unraveled.

High PVP is not always a risk factor for FV bleeding (13,16), and it has been reported that PVP decreased according to the development of GRS (25). These characteristic features in the FV may support the findings that the diameter and FVo of GRS did not show significant difference between bleeders and nonbleeders in the present study. However, our results have shown that the flow velocity of GRS in bleeders was significantly higher than that in nonbleeders. Doppler US might be a novel option for predicting FV bleeding in the clinical course of portal hypertension.

There are some limitations to the present study. First, this is a retrospective study about the hemodynamics of GRS at one time in patients with FV. Changes in the hemodynamics of GRS during the long-term clinical course and their correlation with the endoscopic findings, bleeding of FV, and changes of liver function are aspects of great interest in this field. Second, a single operator performed the US examinations in the present study. Although a constant technique for blood flow measurement

may provide highly reliable results and sufficient intraobserver variability was obtained, interobserver variability would also be an important factor for evaluating the methodology. This needs to be examined in further studies. Third, shunt to the renal vein accounts for the drainage pathway in some portosystemic collateral vessels without forming FV in patients with portal hypertension (26,30,31,35). The clinical value of US examination in these patients should be clarified.

CONCLUSION

Our study clarified that the hemodynamic features of GRS under physiologic conditions using Doppler US in cirrhotic patients with FV. Although a prospective study with a large number of patients is needed, this simple and noninvasive technique might be valuable for the clinical management of FV, assessment of its severity, and bleeding risk.

REFERENCES

1. Sarin SK, Lahoti D, Saxena SP, et al. Prevalence, classification and natural history of gastric varices: A long-term follow-up study in 568 portal hypertension patients. Hepatology 1992; 16:1343–1349.
2. Bosch J, Abraldes JG, Groszmann R. Current management of portal hypertension. J Hepatol 2003; 38:S54–S68.
3. Ryan BM, Stockbrugger RW, Ryan JM. A pathophysiologic, gastroenterologic, and radiologic approach to the management of gastric varices. Gastroenterology 2004; 126:1175–1189.
4. Lubel JS, Angus PW. Modern management of portal hypertension. Intern Med J 2005; 35:45–49.
5. D'amico G, Pagliaro L, Bosch J. The treatment of portal hypertension: A meta-analytic review. Hepatology 1995; 22:332–354.
6. Greenwald BD, Caldwell SH, Hespenheide EE, et al. *N*-2-Butyl-cyanoacrylate for bleeding gastric varices: A United States pilot study and cost analysis. Am J Gastroenterol 2003; 98:1982–1988.
7. Tripathi D, Ferguson JW, Therapondos G, et al. Review article: Recent advances in the management of bleeding gastric varices. Aliment Pharmacol Ther 2006; 24:1–17.
8. Kanagawa H, Mima S, Kouyama H, et al. Treatment of gastric fundal varices by balloon-occluded retrograde transvenous obliteration. J Gastroenterol Hepatol 1996; 11:51–58.
9. Koito K, Namieno T, Nagakawa T, et al. Balloon-occluded retrograde transvenous obliteration for gastric varices with gastrorenal or gastrocaval collaterals. AJR Am J Roentgenol 1996; 167:1317–1320.
10. Akahane T, Iwasaki T, Kobayashi N, et al. Changes in liver function parameters after occlusion of gastrorenal shunts with balloon-occluded retrograde transvenous obliteration. Am J Gastroenterol 1997; 92:1026–1030.
11. Yamagami T, Kato T, Iida S, et al. Change in the hemodynamics of the portal venous system after retrograde transvenous balloon occlusion of a gastrorenal shunt. AJR Am J Roentgenol 2003; 181:1011–1015.
12. Scott J, Dick R, Long RG, et al. Percutaneous transhepatic obliteration of gastro-oesophageal varices. Lancet 1976; 2:53–55.
13. Sanyal AJ, Freedman AM, Luketic VA, et al. The natural history of portal hypertension after transjugular intrahepatic portosystemic shunts. Gastroenterology 1997; 112:889–898.
14. Chau T, Patch D, Chan Y, et al. "Salvage" transjugular intrahepatic portosystemic shunts: Gastric fundal compared with oesophageal variceal bleeding. Gastroenterology 1998; 114:981–987.
15. Barange K, Peron JM, Imani K, et al. Transjugular intrahepatic portosystemic shunt in the treatment of refractory bleeding from ruptured gastric varices. Hepatology 1999; 30:1139–1143.
16. Tripathi D, Therapondos G, Jackson E, et al. The role of the transjugular intrahepatic portosystemic stent shunt (TIPSS) in the management of bleeding gastric varices: Clinical and haemodynamic correlations. Gut 2002; 51:270–274.
17. Boyer T. Transjugular intrahepatic portosystemic shunt: Current status. Gastroenterology 2003; 124:1700–1710.
18. Thomas PG, D'Cruz AJ. Distal splenorenal shunting for bleeding gastric varices. Br J Surg 1994; 81:241–244.
19. Yamamoto J, Nagai M, Smith B, et al. Hand-assisted laparoscopic splenectomy and devascularization of the upper stomach in the management of gastric varices. World J Surg 2006; 30:1–6.
20. Kim T, Shijo H, Kokawa H, et al. Risk factors for hemorrhage from gastric fundal varices. Hepatology 1997; 25:307–312.
21. Akiyoshi N, Shijo H, Iida T, et al. The natural history and prognostic factors in patients with cirrhosis and gastric fundic varices without prior bleeding. Hepatol Res 2000; 17:145–155.
22. Matsumoto A, Kitamoto M, Imamura M, et al. Three-dimensional portography using multislice helical CT is clinically useful for management of gastric fundic varices. AJR Am J Roentgenol 2001; 176:899–905.
23. Ono N, Toyonaga A, Nishimura H, et al. Evaluation of magnetic resonance angiography on portosystemic collaterals in cirrhotic patients. Am J Gastroenterol 1997; 92:1515–1519.
24. Anderson CM. GI magnetic resonance angiography. Gastrointest Endosc 2002; 55:S42–S48.
25. Watanabe K, Kimura K, Matsutani S, et al. Portal hemodynamics in patients with gastric varices: A study in 230 patients with esophageal and/or gastric varices using portal vein catheterization. Gastroenterology 1988; 95:434–440.
26. Kimura K, Ohto M, Matsutani S, et al. Relative frequencies of portosystemic pathways and renal shunt formation through the "posterior" gastric vein: Portographic study in 460 patients. Hepatology 1990; 12:725–728.
27. Grant EG, Tessler FN, Perrella RR. Clinical Doppler Imaging. AJR Am J Roentgenol 1989; 152:707–717.
28. Schmassmann A, Zuber M, Livers M, et al. Recurrent bleeding after variceal hemorrhage: Predictive value of portal venous duplex sonography. AJR Am J Roentgenol 1993; 160:41–47.
29. Ferrara K, Deangelis G. Color flow mapping. Ultrasound Med Biol 1997; 23:321–345.
30. von Herbay A, Frieling T, Haeussinger D. Color Doppler sonographic evaluation of spontaneous portosystemic shunts and inversion of portal venous flow in patients with cirrhosis. J Clin Ultrasound 2000; 28:332–339.
31. Yamada M, Ishida H, Komatsuda T, et al. Portal systemic shunt through the renal vein. Abdom Imaging 2006; 31:701–705.
32. Pugh RN, Murray-Lyon IM, Dawson JL, et al. Transection of the esophagus for bleeding esophageal varices. Br J Surg 1973; 60:646–649.
33. The Japan Society for Portal Hypertension. The General Rules for Study of Portal Hypertension, ed 2. Tokyo, Japan: Kanehara & Co., Ltd. 2004:37–50.
34. Kimura K, Tsuchiya Y, Ohto M, et al. Single-puncture method for percutaneous transhepatic portography using a thin needle. Radiology 1981; 139:748–749.
35. Takayasu K, Moriyama N, Shima Y, et al. Sonographic detection of large spontaneous spleno-renal shunts and its clinical significance. Br J Radiol 1984; 57:565–570.

Cell Tissue Res (2008) 333:17–27
DOI 10.1007/s00441-008-0618-4

REGULAR ARTICLE

Hepatoblast-like cells enriched from mouse embryonic stem cells in medium without glucose, pyruvate, arginine, and tyrosine

Minoru Tomizawa · Yoshiro Toyama · Chizuru Ito · Kiyotaka Toshimori · Katsuro Iwase · Masaki Takiguchi · Hiromitsu Saisho · Osamu Yokosuka

Received: 15 November 2007 / Accepted: 31 March 2008 / Published online: 14 May 2008

Abstract In order to enrich hepatocytes differentiated from embryonic stem cells, we developed a novel medium. Since only hepatocytes have the activity of ornithine transcarbamylase, phenylalanine hydroxylase, galactokinase, and glycerol kinase, we expected that hepatocytes would be enriched in a medium without arginine, tyrosine, glucose, and pyruvate, but supplemented with ornithine, phenylanaline, galactose, and glycerol (hepatocyte-selection medium, HSM). Embryoid bodies were transferred onto dishes coated with gelatin in HSM after 4 days of culture. At 18 days after embryoid body formation, a single type of polygonal cell survived with an enlarged intercellular space and micorvilli. These cells were positive for indocyanine green uptake and for mRNAs of albumin, transthyretin, and α-feto protein, but negative for mRNAs of tyrosine aminotransferase, α1-antitrypsin, glucose-6-phosphatase, and phosphoenol pyruvate carboxykinase. Since cells in HSM were positive for cytokeratin (CK) 8 and CK18 (hepatocyte markers) and for CK19 (a marker of bile duct epithelial cells), we concluded that they were hepatoblasts. They showed weaker expression of CCAAT/enhancer-binding protein (C/EBP)α than fetal liver (18.5 days of gestation) and expression of C/EBPβ at a similar level to that of fetal liver. These data support our conclusion that HSM allows the selection of hepatoblast-like cells.

Keywords Hepatocyte · Differentiation · Ornithine carbamoyltransferase · Galactokinase · Indocyanine green · Mouse (EB5 cell line)

This work was supported by the Tsuchiya Foundation, the Ichiro Kanehara Foundation, and a Research Grant-in-Aid for Scientific Research from Japan Society for the Promotion of Science.

M. Tomizawa (✉) · H. Saisho · O. Yokosuka
Department of Medicine and Clinical Oncology,
Graduate School of Medicine, Chiba University,
1–8–1 Inohana, Chuo-ku,
Chiba City, Chiba 260–8670, Japan
e-mail: nihminor-cib@umin.ac.jp

Y. Toyama · C. Ito · K. Toshimori
Department of Anatomy and Developmental Biology,
Graduate School of Medicine, Chiba University,
Chiba City, Chiba, Japan

K. Iwase · M. Takiguchi
Department of Biochemistry and Genetics,
Graduate School of Medicine, Chiba University,
Chiba City, Chiba, Japan

Introduction

Embryonic stem (ES) cells have shown promise for use in regenerative medicine because they produce various types of cells. If hepatocytes could be produced and enriched from ES cells, they might be transplantable to patients suffering from liver insufficiency or useful as a liver-assist device (Heo et al. 2006; Soto-Gutierrez et al. 2006). To date, various protocols have been reported regarding the differentiation protocol of ES cells to hepatocytes (Lavon and Benvenisty 2005): (1) ES cells can be differentiated to hepatocytes by withdrawal of leukemia inhibitory factor (LIF; Jones et al. 2002); (2) the differentiation of ES cells to hepatocytes is promoted by growth factors, such as hepatocyte growth factor, and extracellular matrix, such as type I collagen (Hamazaki et al. 2001); transcription factor, such as hepatocyte nuclear factor (HNF)-3β, has been

introduced to promote hepatocyte differentiaion from ES cells (Ishizaka et al. 2002). Although some of the cells are positive for genes specific to hepatocytes, others are not. If cells derived from ES cells are transplanted without enrichment of hepatocytes, teratoma will be formed (Teramoto et al. 2005). We therefore need to develop methods to purify hepatocytes differentiated from ES cells.

Hepatocytes differentiated from ES cells are enriched, for fluorescence-associated cell sorting, with green fluorescent protein driven by an albumin promoter as a marker of hepatocytes (Heo et al. 2006). Ethical problems may arise in the application of this method for humans in a clinical setting, since this requires the introduction of foreign genes into humans. Hepatocytes can be successfully enriched by Percoll gradient centrifugation followed by magnetic cell sorting (Kumashiro et al. 2005). One problem of this method is that undifferentiated cells may contaminate hepatocytes. Another problem is that embryoid bodies are difficult to disaggregate, as they are tightly bound by their extracellular matrices. The development of a novel way to isolate hepactocytes from ES cells would therefore be desirable. Since hepatocytes produce metabolites necessary for cells to survive, e.g., via the urea cycle and gluconeogenesis, we expected that a medium lacking their products would enrich hepatocytes from cells differentiated from ES cells.

Endodermal patterning begins in a mouse embryo at the six-somite stage (Zaret 2002). Hepatic genes are induced in a segment of the definitive endoderm at 8.5 days of gestation. Expression of HNF-3β appears in endodermal cells, occupying the promoters of liver-specific genes (Bossard and Zaret 1998). Our method with medium lacking LIF (ESM) is a spontaneous differentiation protocol (Lavon and Benvenisty 2005). Hanging drop culture for 5 days has been used in previous reports, whereas we have employed 4 days in our protocol (Jones et al. 2002; Yamada et al. 2002). Similarly, 15% fetal calf serum (FCS) has been previously used, whereas we have chosen 10% FCS (Miyashita et al. 2002; Abe et al. 1996). Culture periods of 30 days for embryoid bodies on gelatin-coated dishes have been used formerly (Miyashita et al. 2002), but we have selected 14 days for our protocol. Sodium pyruvate has been included in our ESM, since withdrawal of LIF is used for differentiation. In our preliminary experiments, the decrease of cell number when deprived of sodium pyruvate prompted us to speculate that sodium pyruvate inhibited differentiation. Shorter culture in hanging drops and less FCS and sodium pyruvate might inhibit differentiation for the expression of albumin, although cells in ESM differentiate toward endoderm, as evidenced by HNF-3β and Delta like (Dlk)-1. We changed from ESM to hepatocyte-selection medium (HSM) at the same time of transfer of embryoid bodies to gelatin-coated dishes in order to enrich hepatoblast-like cells successfully, whereas cells in ESM remained at more immature state than those in HSM. We did not use any growth factors or extracellular matrix specific to hepatocyte differentiation. We proposed that the change of medium to HSM at 4 days of hanging drop culture would be suitable for ES cells to enrich hepatoblast-like cells. The endodermal cells proliferate and migrate into the septum transversum to form hepatic endoderm in which hepatoblasts appear. After 12 days of gestation, hepatoblasts start to differentiate into hepatocytes or biliary epithelial cells (Lavon and Benvenisty 2005). During hepatoctye differention, the expression of liver-specific transcription factors appears to up-regulate liver-specific genes. One example is that CCAAT-enhancer binding protein (C/EBP) α appears to promote the expression of ornithine transcarbamylase (OTC; Murakami et al. 1990). OTC, mainly expressed in hepatocytes, catalyzes the second step of the urea cycle to produce arginine.

Among all amino acids, withdrawal of arginine is tolerated the least by cultured cells in vitro (Wheatley et al. 2000). Arginine is produced via the urea cycle, which is exclusive to hepatocytes. Indeed, withdrawal of arginine led to the first medium for the purification of hepatocytes (Leffert and Paul 1972). Tyrosine is produced by hepatocytes. Interestingly, a subline of hepatoma cells is established in a medium deprived of serum, arginine, and tyrosine (Niwa et al. 1980). The cell line has the activity of OTC, which is involved in the urea cycle, and phenylalanine hydroxylase (PAH), which produces tyrosine. PAH is distributed in liver and kidney (McGee et al. 1972). Consequently, we might expect that hepatocytes can be enriched from ES cells in a medium without arginine and tyrosine.

Glucose is an important source of energy for the survival of cells. Withdrawal of glucose contributes to the enrichment of hepatocytes since they can produce it (Leffert and Paul 1972). Pyruvate, the final product of glycolysis, enters the citric acid cycle. When pyruvate plus glucose is withdrawn from the medium, all neural cells die (Matsumoto et al. 1994). Pyruvate is produced from phosphoenol pyruvate by pyruvate kinase (PK), expressed in liver, kidney, and red blood cells. Glycerol and galactose enter glycolysis via glycerol kinase (GK) and galactokinase, both of which are expressed in liver and kidney (Ai et al. 1995; Ohira et al. 2005). We therefore expected that hepatocytes would be specifically capable of surviving in the presence of galactose and glycerol and in the absence of either glucose or pyruvate (Phillips et al. 2002; Sumida et al. 2002).

Here, we have investigated whether we can enrich hepatocytes derived from ES cells in medium deprived of arginine, tyrosine, glucose, and pyruvate, and supplemented with ornithine, glycerol, and galactose. Insulin and dexamethasone have to be added, as they maintain primary cultured hepatocytes (Inoue et al. 1989).

Materials and methods

Cell culture, light microscopy, and cell counting

EB5, a cell line of mouse ES cells provided by Dr. H. Niwa (Center for Developmental Biology, Riken, Kobe, Japan), was maintained undifferentiated in dishes coated with gelatin (Sigma Aldrich Japan, Tokyo, Japan) without feeder cells in Glasgow minimum essential medium (GMEM; Sigma Aldrich Japan) supplemented with 10% FCS (Roche Diagnostics, Tokyo, Japan), 1× non-essential amino acids (Invitrogen Japan, Tokyo, Japan), sodium pyruvate (1 mM; Invitrogen), 2-mercaptoethanol (0.1 mM; Wako Pure Chemicals, Osaka, Japan), and LIF (1000 U/ml; Invitrogen; Niwa et al. 2002). To induce differentiation, dissociated ES cells were cultured in hanging drops at a density of 1,000 cells per 30 μl of the above media (based on GMEM) without LIF (ESM) to form embryoid bodies. After 4 days in hanging drop culture, the resulting embryoid bodies were plated onto plastic dishes (Iwaki-Asahi Techno Glass, Tokyo, Japan) coated with gelatin. To isolate hepatocytes differentiated from ES cells, the medium was changed into hepatocyte-selection medium (HSM) on the transfer of embryoid bodies onto dishes coated with gelatin. HSM was originally made from amino acid powders based on L15, deprived of arginine, tyrosine, glucose, or sodium pyruvate, but supplemented with galactose (900 mg/l; Wako), ornithine (1 mM; Wako), glycerol (5 mM; Wako), and proline (260 mM; Wako). Proline was added because of its requirement for DNA synthesis (Nakamura et al. 1984). Aspartic acid was withdrawn, it being one of the products of ornithine and a substrate of arginine. HSM was supplemented with insulin (10 μM; Sigma Aldrich), dexamethasone (10 μM; Wako), aprotinin (5,000 U/ml; Wako), and 2-mercaptoethanol (0.1 mM; Sigma Aldrich). FCS was added at a final concentration of 10% after dialysis against phosphate-buffered saline (PBS) to exclude amino acids and D(+)-glucose. Cells were observed microscopically with an IMT-2 (Olympus, Tokyo, Japan). Three embryoid bodies were transferred onto 6-well plates (Iwaki-Asahi) coated with gelatin and cultured in either ESM or HSM. Cells were washed with physiological saline, harvested with 0.05% trypsin-0.53 mM EDTA (Invitrogen), followed by cell counting by the trypan blue dye (Sigma Aldrich) exclusion test. The cell counting was repeated three times.

Electron microscopy

Grown colonies of hepatocyte-like cells in the culture dishes (Iwaki-Asahi) were selected under light microscopy, and the culture medium was discarded. Colonies remaining in the dish were fixed with 2.5% glutaraldehyde (TAAB, Aldermaston, UK) in HEPES buffer (pH 7.4) for 2 h at room temperature. After being washed gently with the HEPES buffer, the cells were postfixed with 1% osmium tetroxide for 15 min. Then, the cells were dehydrated in a graded ethanol series, immersed in a mixture of ethanol and Epon (1:1) for 15 min, and embedded in Epon.

After polymerization, the Epon disc containing the cell colonies was removed from the culture dish. Colonies of cells for observation were selected under a binocular or inverted light microscope. Sections were cut parallel to the disc surface. Semi-thin sections were stained with toluidine blue for light microscopy, and ultra-thin sections were stained with uranyl acetate and lead citrate for observation under an electron microscope (JEM 1200 Ex II, JEOL, Tokyo, Japan) at 80 kV.

Animals

C57BL/6 mice were housed and mated in animal facilities at Chiba University Graduate School of Medicine, with food and acidified water provided ad libitum. Mice were killed by carbon dioxide under NIH guidelines for proper animal procedures, and livers were snap-frozen in liquid nitrogen for storage in −80°C until the experiments.

Indocyanine green uptake study

Indocyanine green (ICG, 25 mg; Dai-ichi Pharm, Tokyo, Japan) was dissolved in 5 ml water in a sterile vial and added to 20 ml each medium at a final concentration of 1 mg/ml. The ICG solution was added to the cell culture and incubated at 37°C for 15 min (Yamada et al. 2002). After the dish was rinsed with PBS, the ICG uptake was observed under microscopy. The number of ICG-positive cells per 100 cells was counted in five different fields. The counting was repeated three times.

Immunostaining

Embryoid bodies were transferred onto 4-chamber glass slides (Clontech, Mountain View, Calif.) coated with gelatin and were fixed with ethanol 18 days after differentiation. Following inactivation of endogenous peroxidase with 2% hydrogen peroxide in methanol, cells were incubated first with 1:500 diluted rabbit anti-mouse albumin antibody (Cappel, Aurora, Ohio) overnight and then with horseradish-peroxidase-labeled anti-rabbit antibody (GE Healthcare Bio-Sciences, Piscataway, N.J.) at a 1:500 dilution. Color was developed with a Dako Envision Kit (DAKO Japan, Tokyo, Japan). Numbers of albumin-positive cells were counted against 100 cells in five different fields by light microsopy, and the ratio of numbers of albumin-positive cells/numbers of counted cells was

calculated. Adult liver (NIH Swiss) fixed in 4% paraformaldehyde and embedded in paraffin was used as positive control (Merck Japan, Tokyo, Japan).

Reverse transcriptase/polymerase chain reaction

Total RNA (5 μg), isolated with Isogen (Nippon Gene, Tokyo, Japan), was used for first-strand cDNA synthesis with Super Script III and oligo (dT) following the manufacturer's instructions (Invitrogen). The polymerase chain reaction (PCR) was performed with *Taq* DNA polymerase (Applied Biosystems Japan, Tokyo, Japan). The PCR primers, annealing temperature, and number of cycles, and the length of the amplified products were as below: Oct3/4 (GenBank accession no. NM_013633, 5′-TCTTTCCACCAGGCCCCCGGCTC, 5′-TGCGGGCGGACATGGGGAGATCC; 65°C; 30 cycles, 224 bp), Nanog (GenBank accession no. AB093574, 5′-CAGGTGTTTGAGGGTAGCTC, 5′-CGGTTCATCATGGTACAGTC; 50°C; 30 cycles; 223 bp), HNF-3β (GenBank accession no. L10409, 5′-TCAAGTGTGAGAAGCAACTG, 5′-GACGACATGAGGTTGTTGAT; 58°C; 30 cycles; 391 bp), Dlk-1 (GenBank accession no. NM_010052, 5′-ATGCTTCCTGCCTGTGC, 5′-GCACGGGCCACTGGC; 58°C; 30 cycles; 200 bp), transthyretin (TTR; GenBank accession no. BC024701, 5′-CTCACCACAGATGAGAAG, 5′-GGCTGAGTCTCTCAATTC; 55°C; 40 cycles; 225 bp), α-feto protein (AFP; GenBank accession no. BC066206, 5′-TCGTATTCCAACAGGAGG, 5′-AGGCTTTTGCTTCACCAG; 55°C; 40 cycles; 173 bp), albumin (GenBank accession no. BC049971, 5′-GTCTTAGTGAGGTGGAGCAT, 5′-ACTACAGCACTTGGTAACAT; 58°C; 35 cycles; 569 bp), tyrosine aminotransferase (TAT) (GenBank accession no. BC024120, 5′-ACCTTCAATCCCATCCGA, 5′-TCCCGACTGGATAGGTAG; 50°C; 30 cycles; 206 bp), α1-antitrypsin (GenBank accession no. M33567, 5′-CAATGGCTCTTTGCTCAACA, 5′-AGTGGACCTGGGCTAACCTT; 63°C; 30 cycles; 518 bp), glucose-6-phosphatase (G6P; GenBank accession no. U00445, 5′-CAGGACTGGTTCATCCTT, 5′-GTTGCTGTAGTAGTCGGT; 55°C; 40 cycles; 210 bp), phosphoenol pyruvate carboxykinase (PEPCK; GenBank accession no. AF009605, 5′-TCTGCCAAGGTCATCCAGG, 5′-GTTTTGGGGATGGGCACTG; 55°C; 40 cycles; 290 bp), cytokeratin (CK)8 (GenBank accession no. BC094009, 5′-ATCGAGATCACCACCTACCG, 5′-TGAAGCCAGGGCTAGTGAGT; 55°C; 25 cycles; 127 bp), CK18 (GenBank accession no. BC089022, 5′-CGAGGCACTCAAGGAAGAAC, 5′-CTTGGTGGTGACAACTGTGG; 55°C; 25 cycles; 247 bp), CK19 (GenBank accession no. AB033744, 5′-TGATCGTCTCGCCTCCTACT, 5′-CAAGGCGTGTTCTGTCTCAA; 55°C; 25 cycles; 262 bp), γ-glutamyl transpeptidase (G-GTP; GenBank accession no. U30509, 5′-AACTTCATCAAGCCAGGTAAGCAG, 5′-TGACTTCTGTATGGTGGTGCCG; 58°C; 40 cycles; 289 bp), OTC (GenBank accession no. BC024893, 5′-ACTGTCCACAGAAACAGGC, 5′-ATCCAGCTGAGGGTAAGACC; 55°C; 40 cycles; 300 bp), PAH (GenBank accession no. NW 001843471, 5′-TCGCTATGACCCCTACACTC, 5′-GGTTGACCTCCTAAGTTCTG; 58°C; 40 cycles; 167 bp), GK (GeneBank accession no. U48403, 5′-ATCCGCTGGCTAAGAGACAACC, 5′-TGCACTGGGCTCCCAATAAGG; 58°C; 40 cycles; 140 bp), galactokinase (GenBank accession no. AF246459, 5′-CATCACCAACTCCAATGTCCG, 5′-ATGCGACTGCCATAAACCCC; 60°C; 40 cycles; 366 bp), and β-actin (GenBank accession no. NM_007393, 5′-TTCCTTCTTGGGTATGGAAT, 5′-GAGCAATGATCTTGATCTTC; 55°C; 40 cycles; 206 bp).

Northern blot analysis

Total RNA (1 μg) was subjected to electrophoresis in a denaturing formaldehyde-agarose gel and transferred to a nylon filter. Hybridization was performed with a DIG Northern starter kit (Roche) following the manufacturer's instructions. A *Pst*I-*Sst*I fragment from 0.35xbC/EBP, kindly provided by Dr. Kleanthis G. Xanthopoulos (Anadys Pharmaceuticals, San Diego, Calif.), was used as a probe for C/EBPα, and a *Bam*HI fragment from pCDANII/mC/EBPβ as a probe for C/EBPβ. Images were scanned and analyzed with ImageJ 1.34 s (National Institutes of Health, Bethesda, Md.). The intensity of 28S rRNA was used as the internal control. The expression levels of C/EBPα and C/EBPβ were calculated as their signal intensity divided by that of 28S rRNA. The experiments were repeated three times.

Statistical analysis

One-factor analysis of variance was performed for statistical analysis with JMP5.0J (SAS Institute Japan, Tokyo, Japan). A P-value of <0.05 was accepted as statistically significant.

Results

Decrease of colony size in HSM

Our initial goal was to enrich cells differentiating to hepatocytes. In ESM, the colonies grew constantly, and the types of cells varied while forming gland-like structures. In HSM, the size of the colonies did not change significantly until day 14. On day 18, unexpectedly, their size dramatically decreased (Fig. 1f). On day 28, most of the cells in HSM had disappeared, as HSM was not suitable

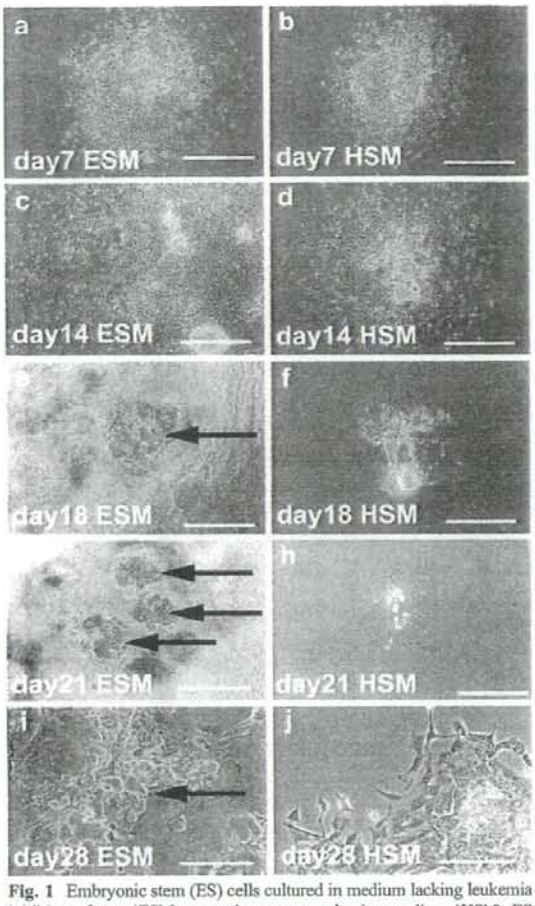

Fig. 1 Embryonic stem (ES) cells cultured in medium lacking leukemia inhibitory factor (*ESM*) versus hepatocyte-selection medium (*HSM*). ES cells were cultured in ESM as embryoid bodies for 4 days, transferred onto dishes coated with gelatin, and then grown in ESM or HSM. **a**, **c**, **e**, **g** Colonies in ESM grew constantly and gland-like structures appeared (*arrows*). **b**, **d**, **f**, **h** Colonies in HSM grew until day 14 but shrank toward day 28. Colonies in ESM consistently contained various types of cells with a gland-like structure (**i**, *arrow*), whereas those in HSM appeared as polygonal cells (**j**). Original magnifications: ×40 (**a**–**h**), ×200 (**i**, **j**). *Bars* 250 μm (**a**–**h**), 50 μm (**i**, **j**)

for their survival (Fig. 1h). Colonies in ESM at day 28 contained gland-like structures (Fig. 1i). Cells surviving in HSM beyond day 18 were uniquely polygonal and were firmly attached to each other (Fig. 1j).

Electron-microscopic analysis

Well-grown colonies of hepatocyte-like cells in culture dishes were selected (Fig. 2a); these cells showed cell division (Fig. 2b) and binuclei (Fig. 2b, inset). Electron-microscopic analysis revealed that most of these cells possessed a large nucleus and scanty cytoplasm (Fig. 2c, d). Interestingly, where three or four cells met, the intercellular space was enlarged and contained short microvilli (Fig. 2c,d). The intercellular connection was held intact during cell division (Fig. 2d). Adherens junctions

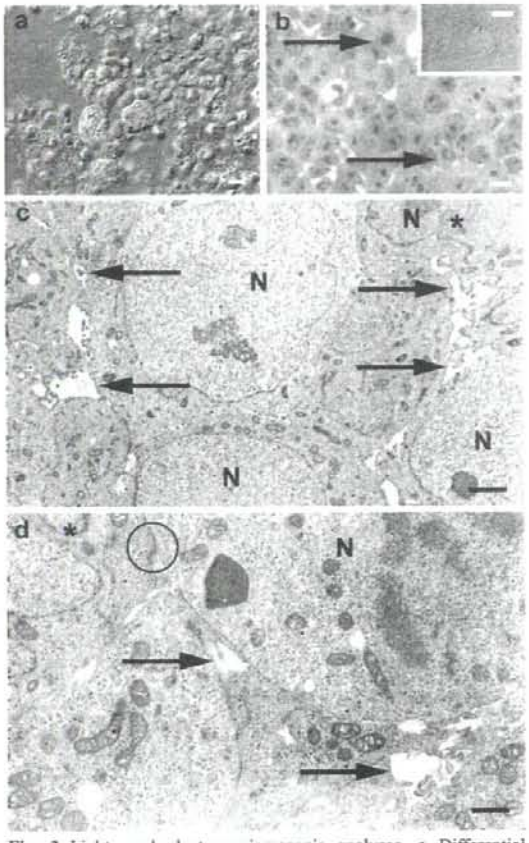

Fig. 2 Light- and electron-microscopic analyses. **a** Differential interference contrast (unfixed) image with Hoechst 33342 staining for live cells (*blue*). **b** Light-microscopic images obtained after toluidine-blue staining (*blue*), corresponding to **a** (*arrows* cells undergoing mitosis). *Inset*: Binucleated cells were sometimes found corresponding to frequent mitosis (*arrows* in **b**). Nuclei were stained with Hoechst 33258. **c**, **d** Electron-microscopic images from a sample similar to the cell mass shown in **a**, **b** (*N* nucleus). Each cell in the colonies possessed a large nucleus and scanty cytoplasm (**c**, **d**). At the point where three or four cells met, the intercellular space was enlarged and contained short microvilli (*arrows* in **c**, **d**). Intercellular connections remained intact during cell division (*circle* in **d**). The nucleus had deep invaginations in many cells (*stars* in **c**, **d**). In higher magnification images (**d** cell division phase), the abundant free ribosomes and a small number of rough endoplasmic reticulum were seen in the cytoplasm. The smooth endoplasmic reticulum was poorly developed. Mitochondria, cytoskeletal components, and Golgi apparatus were well developed. Glycogen was occasionally found. *Bars* 10 μm (**a**, **b**), 5 μm (*inset* in **b**), 1 μm (**c**), 2 μm (**d**)

were found (Fig. 2c), and gap junctions were observed (not shown). Tight junctions were not observed in this study. The nucleus had deep invaginations and prominent nucleoli. The cytoplasm contained abundant free ribosomes and small numbers of rough endoplasmic reticulum. The smooth endoplasmic reticulum was poorly developed. Mitochondria and cytoskeletal components were well developed and at an average level. The Golgi apparatus had also developed normally. Glycogen was not abundantly found in this study.

Cell number

On day 0, 3×10^3 cells were transferred into each well of a 6-well plate (Fig. 3). On day 7 after differentiation, the cell number had increased to $(6.0\pm0.5)\times10^3$ (average±SD) in wells containing ESM, whereas it only showed a slight increase to $(4.1\pm0.4)\times10^3$ in wells with HSM. On day 18, the cell number had increased significantly to $(5.7\pm0.6)\times10^4$ in wells with ESM ($P<0.05$) but had decreased to $(1.1\pm0.2)\times10^3$ in wells with HSM ($P<0.05$). These data clearly showed that only a small number of cells survived in HSM.

ICG uptake and albumin staining

ICG uptake and albumin overexpression are useful hepatocyte markers. ICG was diffusely or granularly detected in the cytoplasm of many cells in HSM (Fig. 4b), whereas only a limited number of cells were ICG-positive in ESM (Fig. 4a): 88±10% of cells in HSM were positive for ICG, but only 1.7±0.2% of cells in ESM were positive for this marker (Fig. 4d). ICG-negative cells were small and polygonal (Fig. 4c). All cells in HSM were strongly positive for albumin in their cytoplasm (100%; Fig. 4h), whereas no cells in ESM were albumin-positive (0%; Fig. 4f). The cytoplasm of hepatocytes of adult liver was positive (Fig. 4j).

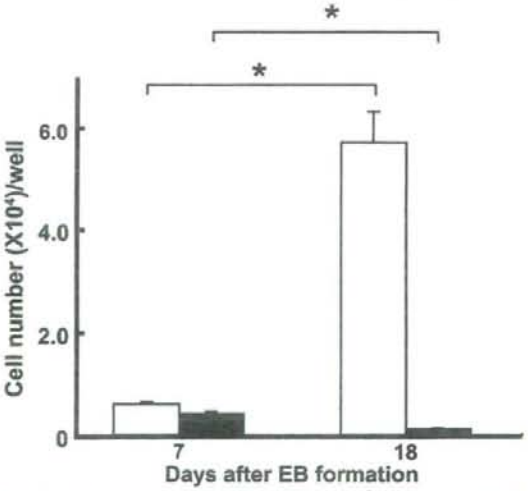

Fig. 3 Cell number in ESM versus HSM: 3×10^3 cells were cultured in each well of 6-well plates coated with gelatin and containing either ESM or HSM. Cell number was counted at 7 and 18 days after formation of embryoid bodies (*EB*). Cell number significantly increased in ESM ($P<0.05$), whereas it apparently decreased in HSM ($P<0.05$). *Open bars* Cell number in ESM, *closed bars* cell number in HSM, *error bar* standard deviation, $^*P<0.05$, $n=3$

Expression of liver-specific genes

We characterized cells in ESM or HSM by reverse transcriptase/polymerase chain reaction (RT-PCR) for the expression of genes specific for hepatocytes (Fig. 5a,b). Oct3/4 and Nanog, markers of pluripotent cells, were positive in ES cells, cells grown in ESM, and those cultured in HSM, but negative in fetal and adult liver. HNF-3β, an endodermal marker, was positive in cells in ESM and HSM, fetal liver, and adult liver. Dlk-1, a hepatoblast marker, was positive in cells in ESM and HSM and fetal liver. TTR and AFP were positive in cells in ESM and in HSM. TAT, α1-antitrypsin, G6P, and PEPCK were negative in cells in both ESM and HSM. Interestingly, albumin mRNA was weakly but still distinctly expressed in cells in HSM and at a marginal level in cells in ESM. CKs are markers of epithelial cells; CK8, CK18, and CK19 were positive in cells in both HSM and ESM. CK19 was negative in adult liver. G-GTP was expressed strongly in ES cells and fetal liver and very faintly in cells in HSM. G-GTP was not expressed in cells in ESM or adult liver. OTC and PAH were negative in cells in HSM and ESM. GK was positive in all samples. Galactokinase and PK were positive in cells in HSM, but negative in those in ESM. We also examined the expressions of C/EBPα and C/EBPβ, liver-specific transcription factors involved in hepatoctye differentiation, by Northern blot analysis. No expression of C/EBPα was observed in cells in ESM, but weak expression was seen in cells in HSM (Fig. 5c). With regard to C/EBPβ, weakly positive expression was observed in undifferentiated ES cells (Fig. 5d), and significantly stronger expression was seen in grown cells in HSM than those cultured in ESM, the expression in HSM being at almost the same level as that in fetal liver. Increased expression of C/EBPα and C/EBPβ compared with adult was a feature consistent with previous reports (Nagy et al. 1994).

Discussion

In preliminary experiments, we cultured embryoid bodies in ESM for 4 days, after which we cultured them in ESM for 21 days when hepatocytes are fully differentiated in mouse

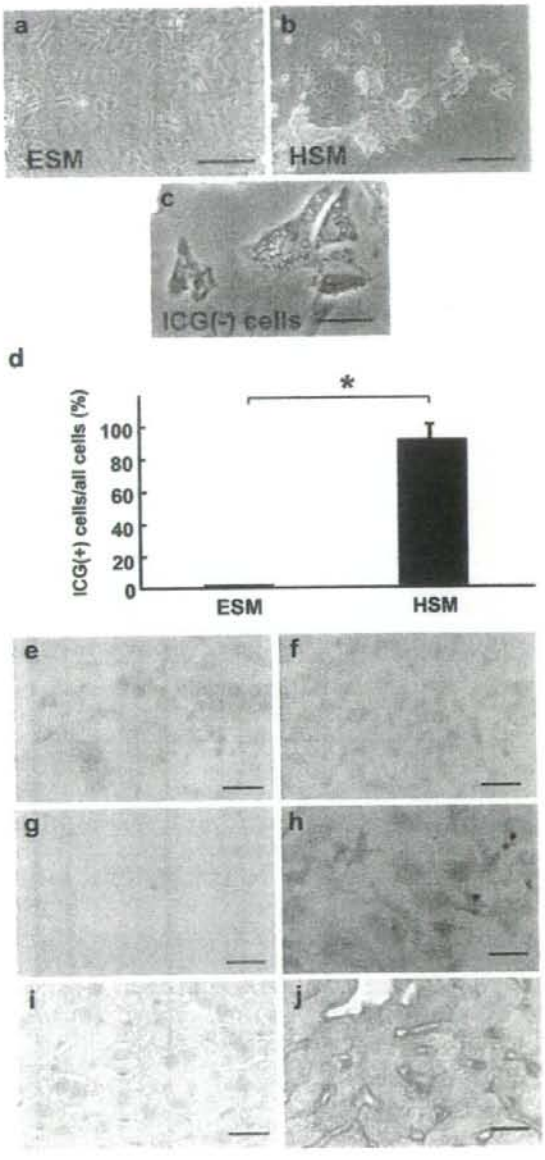

◀ **Fig. 4** ICG uptake and albumin staining. **a–c** At 18 days after the formation of embryoid bodies, 1 mg/ml ICG was added to the medium for 15 min, and the cells were observed microscopically. Most of the cells in HSM (*HSM*) contained fine granules of ICG in their cytoplasm (**b**), but only a small number of cells in ESM (*ESM*) were positive (**a**). ICG-negative cells (*ICG(−)*)were small and polygonal (**c**). **d** Numbers of ICG-positive cells (*ICG(+)*) per 100 cells were counted in five different fields and were significantly higher in HSM than in ESM ($P<0.05$). **e–h** Cells in ESM and HSM were stained with anti-albumin antibody 18 days after the formation of embryoid bodies. The cytoplasm of all cells was strongly positive for albumin in HSM (**h**), but not in ESM (**f**). **j** Positive control: Adult liver was stained with anti-albumin antibody; hepatocytes of adult liver were strongly positive for albumin. **e**, **g**, **i** Negative controls: ES cells in ESM (**e**) or HSM (**g**) 18 days after the formation of embryoid bodies or adult liver (**i**) stained without anti-albumin antibody. Original magnifications: ×50 (**a**, **b**), ×100 (**c**), ×40 (**e–j**). *Bars* 25 μm (**a**, **b**), 5 μm (**c**),

uterus, and then cultured them for 20 days in either ESM or HSM. Three embryoid bodies were spread in wells of 6-well plates (3×10^3 cells). After 20 days of culture in either ESM or HSM with above protocol, each well had 1.3×10^6 cells in ESM but 4.0×10^5 cells in HSM. ICG-positive cells accounted for 1.5% of the cells in ESM but 50% in HSM, suggesting that HSM did not sufficiently enrich cells differentiating to hepatocytes in this protocol. We speculated that cells cultured in ESM for 21 days expressed genes specific to hepatocytes. Day 4 was thus chosen on which to change the medium in order to delete most of the cells, before they acquired the expression of hepatocyte-specific genes. The sizes of the colonies were the same between ESM and HSM until day 14. Suddenly on day 18, the size of the colonies in HSM dramatically decreased. ES cells started to differentiate once LIF was withdrawn, and their function changed constantly. Possibly, they maintained their function to survive HSM with dialyzed serum as nutrition prior to day 14. Beyond day 14, they lost the function, and the surviving cells were those differentiating toward hepatocytes. This hypothesis was supported by the results of RT-PCR. Cells in ESM down-regulated the expression of galactokinase and GK. The disappearing cells were not analyzed because they were degraded and fragmented and were difficult to identify in advance. In the preliminary experiments using 21 days to apply selection, cell numbers decreased, but OTC was negative as revealed by RT-PCR. The percentage of ICG(+) cells was lower. We speculated that (1) on day 4, cells had appeared that were differentiating toward hepatocytes, (2) other cells did not express any of the liver-specific genes. Therefore, we concluded that day 4 was more appropriate for the application of selection pressure. The culture of embryoid bodies in HSM significantly reduced the cell numbers, and 88% of surviving cells were positive for ICG. An enlarged intercellular space and microvilli were observed by electron microscopy. Almost all cells surviving in HSM were positive for albumin. Since ICG uptake and albumin expression are markers of hepatocytes, we concluded that HSM was highly efficient in causing the enrichment of hepatocytes from differentiating ES cells (Teratani et al. 2005; Yamada et al. 2002). Using this method, we did not need to introduce any genes into the ES cells nor manipulate colonies, but simply deprived the medium of ingredients. Our method would thus be safer and more straightforward than previously reported methods, and possible ethical problems could be avoided. We changed ESM to HSM at

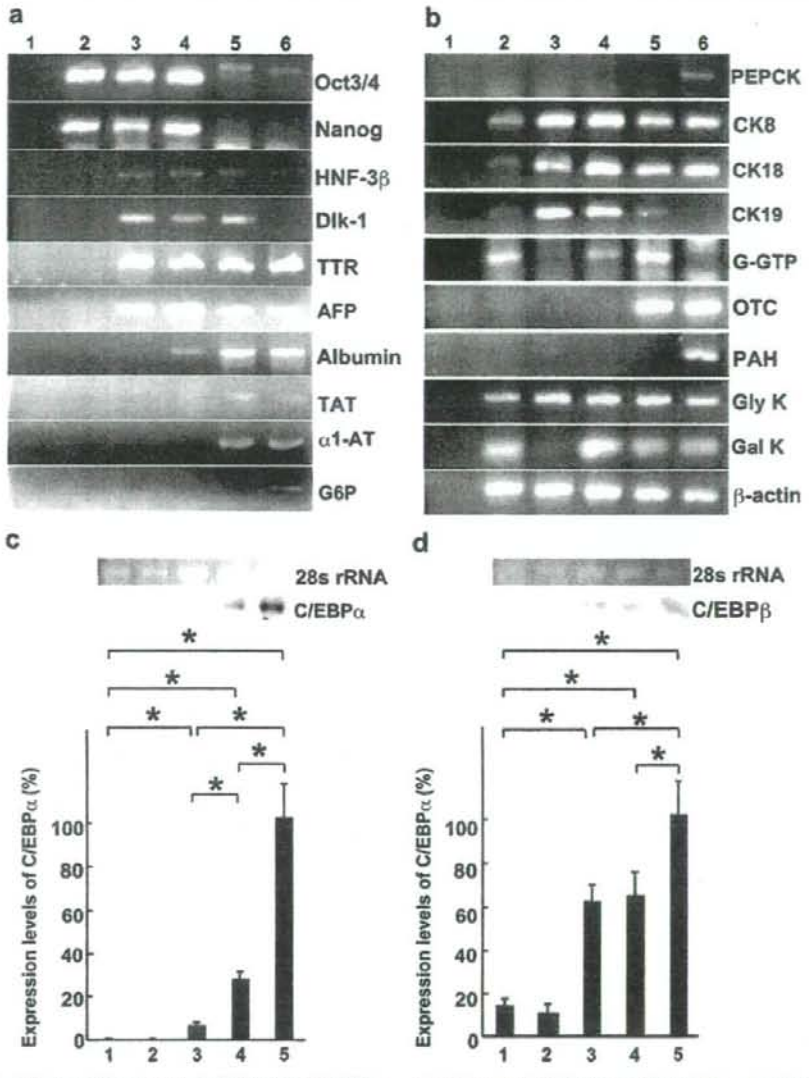

Fig. 5 Expression of liver-specific genes. **a**, **b** RNA was isolated from embryonic stem cells cultured with leukemia inhibitory factor (*lanes 2*), cells cultured in either ESM (*lanes 3*) or HSM (*lanes 4*) 18 days after formation of embryoid bodies, fetal mouse liver at 18.5 days of gestation (*lanes 5*), and adult mouse liver (*lanes 6*). *Lanes 1* Negative control (H_2O). Expression of genes specific for hepatocytes was analyzed with RNA subjected to reverse transcriptase/polymerase chain reaction. Oct3/4, Nanog, HNF-3β, and Dlk-1 were positive in *lanes 3, 4*. *Lane 4* was positive for TTR, AFP, albumin. Interestingly, albumin was not expressed in ESM and only weakly in HSM. CK8, CK18, CK19, and G-GTP were positive in *lane 4*. Note that CK19 and G-GTP were negative in *lane 6*. Galactokinase was positive in *lane 4* but negative in *lane 3* (*TTR* transthyretin, *AFP* α-feto protein, *TAT* tyrosine aminotransferase, *α1-AT* α1-antitrypsin, *G6P* glucose-6-phosphatase, *G-GTP* gamma-glutamyl transpeptidase, *OTC* ornithine transcarbamylase, *PEPCK* phosphoenol pyruvate carboxykinase, *PAH* phenylalanine hydroxylase, *Gly K* glycerol kinase, *Gal K* galactokinase). **c**, **d** C/EBPα and C/EBPβ are hepatocyte-specific transcription factors. Their expression was analyzed by Northern blotting (*lane 1* cells in a medium with LIF, *lane 2* cells in ESM, *lane 3* cells in HSM, *lane 4* fetal mouse liver, *lane 5* adult mouse liver). C/EBPα was not expressed in cells cultured in ESM but was weakly expressed in HSM (**c**). C/EBPβ was expressed in HSM at almost the same level as in fetal liver at 18.5 days of gestation (**d**). The difference between ESM and HSM was significant for C/EBPα (*P<0.05, n=3; **c**). C/EBPα and C/EBPβ were more strongly expressed in adult liver than in fetal liver at 18.5 days of gestation (*P<0.05, n=3; **c**, **d**)

the same time as the transfer of embryoid bodies to gelatin-coated dishes and successfully enriched hepatoblast-like cells, whereas cells in ESM remained at a more immature state than those in HSM. We did not use any growth factors specific or extracellular matrix specific to hepatocyte differentiation. We therefore propose that the change of the medium to HSM at 4 days in hanging drop culture is a suitable method for enriching hepatoblast-like cells from ES cells.

Our method with ESM is a spontaneous differentiation protocol (Lavon and Benvenisty 2005). Hanging drop culture for 5 days was used in previous reports, whereas we employed 4 days (Jones et al. 2002; Yamada et al. 2002). Moreover, we used 10% FCS, instead of 15% FCS (Abe et al. 1996), and 14 days of culture of embryoid bodies on gelatin-coated dishes instead of 30 days (Miyashita et al. 2002). Our ESM contained sodium pyruvate, whereas HSM did not, with the apparent promotion of hepatocyte differentiation. Shorter culture in hanging drops, lower levels of FCS, and sodium pyruvate might delay the differentiation of the expression of albumin, although cells in ESM differentiated toward endoderm, as evidenced by the presence of HNF-3β and Dlk-1. The variances in the spontaneous differentiation between our ESM and others might be attributable to a difference in karyotype spectrum, which remains to be determined. We attempted to analyze the karyotype of EB5 but failed because we could not obtain appropriate chromosome spreads in orderly arrangements (Longo et al. 1997).

We next characterized cells surviving in HSM for the expression of genes specific for hepatocytes. Cells should ideally be cultured long-term to allow them to differentiate into more mature or fully differentiated hepatocytes as measured by functional assays, such as urea synthesis. Longer-term culture was however impossible, since cells gradually disappeared beyond 18 days of culture in HSM (Fig. 1f). Expression was therefore analyzed with liver-specific genes. Oct3/4 and Nanog were positive in ESM and HSM but negative in fetal and adult liver. Since Oct3/4 and Nanog are positive in endoderm and in cells more immature than those in fetal liver, cells in ESM and HSM might have differentiated to endodermal cells or hepatoblast-like cells (Jones et al. 2002; Yoshida-Koide et al. 2004). HNF-3β and Dlk-1 were positive in ESM and HSM suggesting that cells in ESM and HSM at least differentiated to a point somewhere between endodermal cells and hepatoblasts. Cells in HSM and ESM were positive for TTR, a visceral endodermal marker, and AFP, an early differentiation marker of hepatocytes (Shiojiri et al. 2004). They were, on the other hand, negative for α1-antitrypsin, G6P, and PEPCK, markers of mature hepatocytes (Hamazaki et al. 2001). Electron microcopy showed that a small number of cells were binuclear, a character of hepatocytes, whereas light microscopy revealed that most of the cells had single nuclei. We speculated that cells in HSM were composed of hepatoblast-like cells in the majority, with mature hepatocytes occurring in small numbers. The RNA of binuclear cells might not have been sufficient to give positive results for α1-antitrypsin, G6P, and PEPCK in RT-PCR. Cells in HSM were obviously more mature than those in ESM, since the former were positive for albumin, whereas the latter were negative, as shown by RT-PCR and immunostaining. Immunoreactivity of albumin progressively increases in parallel with hepatocyte differentiation (Gelly et al. 1991). The albumin expression was stronger in adult liver than cells in HSM as shown by RT-PCR, presumably because the former are more mature than the latter. One possibility was that the cells in HSM or ESM were similar to those of yolk sac or undifferentiated endoderm. Our data clearly showed that they were positive for CK8, CK18, CK19, and G-GTP. Since cytokeratins are markers of epithelial cells, cells in HSM were thought to be differentiated beyond yolk sac or endoderm (Barak et al. 2004). Interestingly, CK19 and G-GTP were negative in adult liver, consistent with previous reports (Ichinose et al. 1989; Ikeda and Taniguchi 2005). On the other hand, CK19 and G-GTP have been reported to be expressed in bile duct epithelial cells (Ichinose et al. 1989; Ikeda and Taniguchi 2005). Since hepatoblasts have the characteristics of both hepatocytes and bile duct epithelial cells, the cells selected in HSM are more likely to have been hepatoblast-like cells (Shiojiri et al. 1991; Shiojiri 1997). Interestingly, electron-microscopic analysis has suggested the formation of bile canaliculi with enlarged intercellular space and microvilli. The expression of C/EBPα and C/EBPβ has been described on 9.5 days of gestation in liver premordium and 15.5 days in liver, respectively (Shiojiri et al. 2004; Nagy et al. 1994). Our Northern blot analysis has shown that C/EBPα is negative in cells in ESM but weakly positive in those in HSM. C/EBPβ is positive in cells in HSM at the same level as that in fetal liver (18.5 days of gestation). Since both genes are deeply involved in the expression of liver-specific genes, these data support our conclusion that HSM successfully "purifies" hepatoblast-like cells.

Unexpectedly, OTC and PAH were not expressed in cells in HSM, which was deprived of arginine and tyrosine in order to select cells expressing these enzymes. This result might be attributable to the production of arginine, as protein degradation and reutilization of amino acid are accelerated without arginine (Bradley 1977). Thus, the withdrawal of arginine and tyrosine is not enough to enrich hepatocytes differentiated from ES cells.

Galactose and glycerol were probably sources of pyruvate for cells in HSM, based on the finding that galactokinase and GK were expressed. Galactokinase was down-regulated when cells differentiated in ESM. The